Ice phases under ambient and high pressure: Insights from density functional theory

Yuan Fang, Bing Xiao, Jianmin Tao, Jianwei Sun, and John P. Perdew

Phys. Rev. B **87**, 214101 — Published 5 June 2013

DOI: 10.1103/PhysRevB.87.214101

Ice phases under ambient and high pressure: Insights for density functional theory

Yuan Fang, Bing Xiao*, Jianmin Tao, Jianwei Sun* and John P. Perdew*

Department of Physics and Engineering Physics, Tulane University, New Orleans, LA 70118

Abstract

Water is common and plays a crucial role in biological, chemical, and physical processes, but its crystalline or ice state has a complicated structure. In this work, we study the lattice mismatch challenge for ice nucleation on silver iodide, the sublimation energy for different ice phases, and the structural phase-transition pressures of ice, with various density functionals. Our calculations show that the recently-developed MGGA_MS (meta-GGA made simple) yields a lattice mismatch (3%) of ice-Ih with β-AgI in good agreement with experiment (2%), significantly better than the PBE (Perdew-Burke-Ernzerhof) GGA mismatch (6%). MGGA_MS is a computationally efficient semilocal functional that incorporates intermediate-range van der Waals interaction. It is found here to perform well overall for ice, and may be expected to improve upon PBE for liquid water. While MGGA_MS predicts the most realistic volumes and volume changes in the phase transitions of ice-Ih to ice-II and -VIII, a more accurate description of some other properties of the higher-pressure phases (ice-II and -VIII) is provided by some functionals that include long-range van der Waals corrections (e.g., revTPSS+vdW for sublimation energy, and optB88-vdW for transition pressure).

I. Introduction

The structure of liquid water is still under debate[1]. Ice is a molecular crystal formed from water molecules. It exhibits a complex phase diagram [See Fig. 1] with a hexagonal ice-Ih structure under ambient conditions. Ice-Ih is the most common ice phase on the Earth's surface. Because of its relevance to human activities, ice has been widely studied both experimentally and theoretically. Ice is a molecular crystal with intermolecular interaction arising from hydrogen bonds and relatively weaker but important van der Waals (vdW) interactions[2]. An accurate description of its properties requires[2,3] the proper treatment of these intermolecular interactions, over a range of pressures and temperatures, as can be seen in the phase diagram[4]. With the development of new density functionals and vdW dispersion corrections, density functional theory has become a method of choice for a broad class of problems.

Kohn-Sham density functional theory (KS-DFT)[5] is an efficient computational method that is widely used in condensed matter physics and quantum chemistry. The only unknown part of KS-DFT is the density functional for the exchange-correlation (xc) energy, which must be approximated. A semilocal density functional $E_{xc}[n_\uparrow, n_\downarrow]$ has the form [6]

$$E_{xc}[n_\uparrow, n_\downarrow] = \int d^3r n\varepsilon_{xc}(n_\uparrow, n_\downarrow, \nabla n_\uparrow, \nabla n_\downarrow, \tau_\uparrow, \tau_\downarrow) \ , \qquad (1)$$

where $n(\mathbf{r}) = n_\uparrow(\mathbf{r}) + n_\downarrow(\mathbf{r})$ is the total electron density, ε_{xc} is the approximated exchange-correlation energy per electron,

$$\tau_\sigma(\mathbf{r}) = \frac{1}{2}\sum_i^{occu.} |\nabla \emptyset_{i\sigma}(\mathbf{r})|^2 \qquad (2)$$

is the orbital kinetic energy density of spin-σ electrons, and the $\emptyset_{i\sigma}(\mathbf{r})$ are the occupied Kohn-Sham orbitals. The local spin density approximation (LSDA) retains only the local spin density arguments in Eq. (1), while the generalized gradient approximation (GGA) includes the

spin-density gradients, and the meta-GGA further includes the kinetic energy density.

While the exact general form of E_{xc} remains unknown, many exact conditions on E_{xc} have been discovered. Density functional approximations can be developed to satisfy these known conditions, or to fit data sets, or both. Many authors have employed DFT with the generalized gradient approximation[7,8](GGA) to study the properties of liquid water and ice. Popular GGA functionals are less useful where vdW interactions are important[9], and this can explain why certain GGAs underestimate the density of liquid water[10] (PBE by 15%, revPBE[11] by 30%) and the sublimation energy for high-pressure ice[2] (PBE by 15% for ice VIII) compared to experiment. As a result, new functionals which more accurately describe both hydrogen bonds and vdW interactions are strongly needed. The meta-GGA[12] is a natural way to improve accuracy further by making use of additional semilocal information (e.g., the Laplacian of the density and/or the kinetic energy density $\tau_\sigma(\mathbf{r})$). Previous tests showed that meta-GGAs yield better results than GGAs for covalent, ionic, and metallic solids, including atomization energy, lattice constant, bulk modulus, and cohesive energy[13]. Recently, by studying the effect and importance of the dependence of meta-GGA functionals on the kinetic energy density through the dimensionless inhomogeneity parameter[14] $\alpha = (\tau - \tau^W)/\tau^{unif}$ (where $\tau(\mathbf{r}) = \frac{1}{2}\sum_{i\sigma}^{occu.}|\nabla\emptyset_{i\sigma}(\mathbf{r})|^2$ is the positive orbital kinetic energy density, $\tau^W = \frac{1}{8}|\nabla n|^2/n$ is the von Weizsaecker kinetic energy density, and $\tau^{unif} = \frac{3}{10}(3\pi^2)^{2/3}n^{5/3}$ is the kinetic energy density of the uniform electron gas), a new meta-GGA functional MGGA_MS[14] was constructed. MGGA_MS, as used here, does not involve parameters fitted to experiment, Later, two parameters in MGGA_MS, that control its dependence on the density gradient and kinetic energy density, were relaxed to fit to training sets of molecular formation energies and

barrier heights, leading to MGGA_MS2[15] (where "2" stands for two fitting parameters). MGGA_MS2 improves significantly the heats of formation of molecules, while retaining good performance for weak interactions, although slightly worse than that of MGGA_MS. The good performance of MGGA_MS and MGGA_MS2 on weak interactions can be ascribed to the fact that they employ only the dimensionless parameter α to recognize all types of orbital overlap (covalent, metallic, and weak bonds), and extrapolate monotonically from $0 \leq \alpha \leq 1$ to large α[16]. Since weak interactions (hydrogen bonds and van der Waals interactions) are dominant in ice, we choose MGGA_MS to represent this family. Motivated by these observations, we apply several meta-GGA[17] functionals to study the lattice mismatch problem[18] of ice-Ih with β-AgI, the sublimation energy in three different phases of ice, and the structural phase transition pressures of ice.

Because semilocal density functionals are unable to describe the long-range part of the van der Waals interaction, several long-range vdW corrections have been invented. In our work, we apply two of them, the DFT+D2[19] and vdW-DF[20] methods, as benchmarks for our meta-GGA results.

In this paper, we study the performance of GGA and new meta-GGA functionals (including TPSS[6], revTPSS[13], and MGGA_MS[14]) on geometry, sublimation energy, and transition pressures of various ice phases at absolute-zero temperature, without zero-point vibrational effects. Furthermore, by comparing these results with the ones from density functionals corrected for long-range vdW interaction (such as TPSS+D2[19], optB88-vdW[2122] and optB86b-vdW[23]), we aim to understand the advantages and limitations of all these approximations and the extent to which they account for the contributions of hydrogen bonding

and van der Waals interaction. As we will see later, meta-GGA functionals reduce the lattice mismatch value of ice-Ih and β-AgI from 6% (PBE) to around 3%, reasonably close to experiment. Additional calculations for high-pressure ice phases indicate that the older meta-GGAs TPSS and revTPSS still have trouble with vdW forces while the newer MGGA_MS is able to describe these interactions well. However, by adding the appropriate long-range vdW corrections for solids, revTPSS also tends to work well for the high-pressure phases.

II. Computational details

The Vienna Ab initio Simulation Package (VASP)[24,25] in version 5.2.12 has been used for the DFT calculation. VASP is a plane-wave code within the projector augmented wave (PAW) method. The "hardest" PAW potentials available for H and O atoms were used for the sake of high accuracy in the presence of short O-H bonds[18]. Ice-Ih was modeled using Bernal-Fowler's proton-ordered, twelve-water-molecule periodic model[26]. Ice-II and ice-VIII structures were obtained from experiment: twelve molecules in a trigonal cell for ice-II[27] and eight molecules in a tetragonal cell for ice-VIII[28]. The energy of the isolated water molecule was calculated within a $10\times11\times12$ $Å^3$ box. In a convergence test with the PBE and TPSS functional for ice-Ih, the total energies were computed with the kinetic energy cutoff increasing from 900 eV to 1400 eV and the Brillouin zone k-mesh from $2\times2\times1$ to $4\times4\times4$. Based on these tests, the optimizations for three ice crystal geometries and total energies were performed for each functional using a plane wave basis with a kinetic energy cutoff of 1200 eV and a $4\times4\times2$ k-mesh to ensure convergence. All our calculations were self-consistent. The c/a lattice-constant ratios were set to their experimental values, since the supplemental

information of Ref. [2] says that optimizing these ratios affected the volume per molecule negligibly (by less than 0.02 $Å^3/H_2O$ for ice-VIII).

Two long-range van der Waals correction methods are used. First is the DFT+D2 approach of Grimme[19], in which these corrections are described via a simple pair-wise force field and added to the conventional Kohn-Sham DFT energy. The D2 dispersion correction is

$$E_{disp} = -\frac{s_6}{2}\sum_{j\neq i}\sum_{i=1}\frac{C_6^{ij}}{R_{ij}^6} f_{damp}(R_{ij}) \qquad (3)$$

where s_6 is a global scaling factor, C_6^{ij} is the dispersion coefficient for atom pair i j, R_{ij} is the inter-atomic distance, and f_{damp} is a damping function to avoid singularity at R=0. Only TPSS+D2 is included in our work, because the parameters for other meta-GGAs have not been fitted yet. Second is the vdW-DF method proposed by Dion et al.[20] It includes a nonlocal vdW correlation functional added to a semilocal xc energy:

$$E_{xc} = E_x^{GGA} + E_c^{LSDA} + E_c^{nl} \qquad (4)$$

where E_x^{GGA} is the exchange energy of a certain GGA functional, E_c^{LSDA} is the local spin-density approximation (LSDA) to the correlation energy, and E_c^{nl} is the approximate nonlocal energy term. optB88-vdW and optB86b-vdW as used in our work are based on the vdW-DF approach with Becke88 and Becke86 GGA exchange functionals optimized to work with the correlation part[21,22].

III. Results and Discussion

A. Lattice mismatch challenge for ice-Ih and β-AgI

When two materials with different lattice constants are brought together by deposition of one material on another, the lattice mismatch is defined as

$$f = \frac{a_1 - a_2}{0.5\times(a_1 + a_2)} \qquad (5)$$

where a_1 and a_2 are the lattice constants for the two separated materials. Lattice mismatch is a critical parameter for thin film growth on a crystal. For example, large lattice mismatch will prevent the growth of a defect-free epitaxial film unless the thickness of the film is below a certain critical thickness[29]. Consequently, good prediction for lattice mismatch is important for theoretical simulation of such phenomena. For example, crystalline β-AgI is widely used to produce artificial rainfall, because β-AgI smoke provides seed crystals in clouds for rain-inducing ice crystallization[30]. This application is based on the fact that the mismatch between the lattice constants of ice-Ih and crystalline β-AgI is only about 1% at 273 K (~2.2% [18]after extrapolating to low temperature at 10-30 K). However, Feibelman[18] pointed out that the lattice constants of ice-Ih and β-AgI as predicted by LSDA[31] and some GGA-level density functionals produce a significantly too-large mismatch value (~8% for LSDA,~6% for PBE) compared to experiment. This so-called lattice mismatch puzzle led to doubts about using DFT approximations for water-material interactions. Ice-Ih has a hexagonal crystal structure, in which hydrogen bonds constitute about 90% of the whole interaction[2]. On the other hand, β-AgI is a solid with strong van der Waals interactions because of the heavy I^- ions. Therefore, to get an accurate mismatch value, the functional should be able to describe both the hydrogen bond and the dispersion interaction simultaneously, a challenge for most semilocal density functionals.

The first four rows of Fig. 2 show the relative errors for lattice constants and also the lattice mismatch computed from four widely-used GGA functionals. Among them, PBE gives relatively small errors for both structures, but, because of the opposite directions of the errors, the mismatch value calculated by PBE is too large. Conversely, revPBE finds the smallest

mismatch among GGAs, but overestimates the lattice constants for both solids too much. It is known that PBE overestimates hydrogen bonding and fails for the vdW interactions[2]. This explains why PBE overbinds ice-Ih while underbinding β-AgI.

We now discuss the results computed by meta-GGA functionals, the older TPSS and revTPSS and the newer MGGA_MS. We also present the results of three functionals with long-range vdW corrections: TPSS+D2[19], optB88-vdW[21] and optB86b-vdW[23]. From Fig. 2, we can see that, except for TPSS which performs similarly to PBE, the other two meta-GGAs show good agreement with experiment: The relative errors for ice lattice constants are smaller than 1% while the lattice mismatches are around 3% compared to the experimental value of 2.3%. This indicates that these meta-GGAs have the potential to better describe the ambient ice structure.

On the other hand, all functionals with long-range vdW correction give as large a mismatch value as the GGAs do. Fig. 2 shows that, although these functionals give accurate results for β-AgI, they underestimate the lattice constants of ice-Ih more than 2%, worse than PBE. This shows that, by including the long-range vdW corrections in these density functionals, one achieves more accurate results for solids with strong vdW interactions, but less accurate results in ice structures with hydrogen bonds.

Based on these results, the meta-GGA functionals revTPSS and MGGA_MS show the best performance overall. However, as vdW interactions play only a minor role in ice-Ih, studies of properties for different ice phases are needed to understand the ability of various functionals to describe hydrogen bonds and van der Waals interactions in ice.

B. Sublimation energy for ice phases under ambient and high pressure

As mentioned before, solid ice exhibits a rich and complex phase diagram. We next report our tests on ice-Ih at ambient pressure, and on two other proton-ordered phases, in order of increasing pressure: ice-II[27] and ice-VIII[28] (shown in Fig. 1) using GGAs, meta-GGAs, and semilocal functionals with vdW correction. We also compare our computed results with experiment. Previous work[2] indicates that, for the phases at higher pressures, hydrogen bond strengths decrease significantly because the nearest-neighbor water-water distances increase in comparison with those of ice-Ih and the hydrogen bonds twist due to configuration distortions[32]. At the same time, vdW interactions increase because layers of water molecule are packed much closer. Thus the vdW interactions play a more crucial role in determining the properties of ice structures at higher pressure.

Next we discuss the sublimation energies for these three ice phases with different functionals. The sublimation energy is defined as the difference between the energy of an isolated water molecule and the energy per water molecule in the solid structure. It represents the energy change from the solid to the gas phase, including all the intermolecular interactions in the solid structure. For ice structures, intermolecular interactions consist of hydrogen bonds and vdW dispersion forces. By comparing the results for various ice phases, we can analyze the performance of DFT for these two weak interactions. Table I shows the computed results of sublimation energies from various functionals. The total-energy difference ($\Delta U = U - U_{Ih}$, where $U = U_{II}$ or U_{VIII}) with respect to the ice-Ih phase is calculated for high-pressure phases and the results are shown in parentheses. Experiment shows that ice-II is almost as stable as ice-Ih with ΔU only about 1 meV/molecule, while ice-VIII is less stable than ice-Ih by 33 meV/molecule. From Table I, PBE slightly overestimates the sublimation energy for

ice-Ih, while underestimating it by 40 meV/molecule for ice-II and by 117 meV/molecule for ice-VIII. The main reason has been explained by previous work.[2] TPSS and revTPSS yield acceptable sublimation energy for ice-Ih, but still fail for high-pressure phases. The revTPSS total energy difference between ice-VIII and ice-Ih is about 5 times larger than experiment due to underestimation of the sublimation energy for high pressure. Since vdW interactions become stronger with increasing pressure, this indicates that these semilocal functionals do not describe vdW well. Therefore, we also show the sublimation energy of the TPSS+D2[19] method, which is the TPSS meta-GGA with long-range vdW correction. From Table I, we notice that, with the vdW correction, total energy differences (ΔU) are greatly improved compared to GGAs, giving ΔU values much closer to experiment. However, we still notice that the sublimation energies predicted by TPSS+D2 are significantly too large, with mean absolute relative error up to 16%. The strong overbinding can lead to a poor description for structural properties like volume. As we already found in part I and also in Fig.4 (a), TPSS+D2 underestimates the equilibrium volume for all three phases. The DFT+D2 method is constructed for molecules and clusters[19], and seems to over-count the vdW interactions in solid. This phenomenon can also be found within the vdW-DF method, as we can see for optB88-vdW in Table I.

For lack of an accurate vdW correction for solid ice, we employed the vdW data from Ref. [2] which adds the influence of vdW interactions within the scheme of Tkatchenko and Scheffler[33], as calculated to correct the PBE0 hybrid functional. Since this method has been shown to be largely independent of the employed DFT approximation[33] and works well for solids[34], we add this correction to our meta-GGA revTPSS result, and find that the total energy

yields precise sublimation energies (with MARE of 3.5%) and a significant improvement for ΔU. However, for the super high-pressure phase ice-VIII, this revTPSS+vdW predicts an energy difference ΔU (~75 meV) slightly worse than optB88-vdW (26 meV), in comparison to experiment (33 meV), but still performs better than the PBE GGA (177 meV). Finally, the new MGGA_MS works well and performs quite similarly to the revTPSS+vdW with 4.3% MARE and with 70 meV ΔU for ice-VIII. MGGA_MS has no long-range vdW correction, and seems to capture part of the vdW interaction in ice by itself.

C. Transition pressure between ice phases

To better understand how functionals perform for van der Waals interactions, we go on to study the ice phase transitions under pressure, computing the phase transition pressure between ice-Ih and ice-II or ice-VIII. Our calculations are for a static lattice, without zero-point expansion (ZPE). Lacking experimental volumes with the ZPE removed, we used instead Diffusion Monte Carlo (DMC) values from Ref [2] as the reference values, since these DMC calculations are stated to be without ZPE and highly accurate for weak interactions, including vdW-bonded systems[2].

Fig.3 (c) shows the energy versus volume curve for ice-Ih and -VIII phases for MGGA_MS, fitted by the Birch-Murnaghan equation of state [35] :

$$\mathrm{E(V)} = E_0 + \frac{\mathrm{B_0}V}{\mathrm{B_0'}}\left(\frac{\left(\frac{\mathrm{V_0}}{\mathrm{V}}\right)^{\mathrm{B_0'}}}{\mathrm{B_0'}-1} + 1\right) - \frac{\mathrm{B_0V_0}}{\mathrm{B_0'}-1} \qquad (5)$$

where $\mathrm{V_0}$, E_0, and B_0 are the equilibrium volume, total energy, and bulk modulus, and $\mathrm{B_0'}$ is the pressure derivative of the bulk modulus. The equilibrium volume, lattice energy, and bulk modulus for each phase are also obtained from the same EOS parametric fitting, and the results for volume and energy are illustrated in Fig. 3 (a) & (b). Then the transition pressure can be

obtained by constructing the common tangent line (dotted line in Fig. 4 (c)) for the two EOS-fitted energy-volume curves.

We apply this approach with the tested functionals to get the transition pressures from ice-Ih to -II or -VIII, and the results are given in Fig.3 (d). The horizontal axis shows the transition pressure P_{tr} for Ih to II, and the vertical axis shows P_{tr} for Ih to VIII. Because the ice-Ih and -II phases are almost equally stable, the transition pressure is quite small (~0.02 GPa), and only optB88-vdW and MGGA_MS give reasonable predictions. All other functionals predict a transition pressure larger than DMC. For ice-VIII, where the experimental value is 0.44 GPa, optB88-vdW still gives the best result while other functionals with vdW corrections and MGGA_MS also work well. From Fig. 3 (d) for the transition pressure P_{tr}, and from Fig. 3 (b) for the energy difference ΔU , we can see a grouping: vdW-corrected functionals cluster in a close range around experiment and DMC, while GGAs, TPSS and revTPSS fall farther away from this range. Clearly, adding the vdW correction contributes to the improvement of transition properties. Also, notice that the MGGA_MS results fall in the close range with these vdW-corrected functionals. This indicates that MGGA_MS captures at least part of the vdW interactions in ice.

IV. Conclusions

In summary, we have studied hydrogen bond and van der Waals interactions within various ice structures using different density functionals. First we found that two meta-GGA's, revTPSS and MGGA_MS, essentially solve the GGA lattice mismatch puzzle[19] for ice-Ih on β-AgI, and we argued that only a functional like MGGA_MS, that reliably describes intermediate-range van der Waals interaction as well as the hydrogen bond, can reliably solve

this kind of problem.

Then we found that meta-GGA yields a better description than GGA for the sublimation energy and equilibrium volume of low-pressure ice phases, a difficult problem for semilocal functionals. In particular, meta-GGA can describe these properties at least as accurately as vdW-corrected GGAs can, even without relying on vdW dispersion corrections, as demonstrated for MGGA-MS: The results (especially the volume per molecule) for ice-Ih, –II, and -VIII are in quite good agreement with experiment, while the sublimation energy for ice-VIII is slightly underestimated but still improved over GGAs.

We find that MGGA_MS is an accurate method for computing ambient and high-pressure phases of ice, although it needs a long-range vdW correction under super-high pressure. This correction might be of the Grimme type[19], which starts from a long-range expression like $-\frac{C_6}{R^6}$ and then cuts off the short-range or small-R contribution. The cutoff radius, from fits to data for van der Waals bonded complexes, would be longer for MGGA_MS than for most other semilocal functionals.

We have argued elsewhere[15] that MGGA_MS has the right dimensionless ingredients to recognize covalent, metallic, and weak bonds. Other meta-GGAs can be built from these dimensionless ingredients[15], and improved long-range vdW[36,37] corrections might be constructed for them. Such functionals may be useful for many problems, including the problems of liquid water and of DNA/RNA [16].

Acknowledgments: We thank A. Ruzsinszky for pointing out Ref. [3] to us. This work was supported in part by the National Science Foundation under Grant No. DMR08-54769 and by

NSF Cooperative Agreement No. EPS-1003897 with further support from the Louisiana Board of Regents. The computations were made with the help of the Louisiana Optical Network and the Tulane Center for Computational Sciences.

* address after July 1,2013: Department of Physics, Temple University, Philadelphia, Pennsylvania 19122, USA

References

1 A. Møgelhøj, A. K. Kelkkanen, K. T. Wikfeldt, J. Schiøtz, J. J. Mortensen, L. G. M. Pettersson, B. I. Lundqvist, K. W. Jacobsen, A. Nilsson, and J. K. Nørskov, J. Phys. Chem. B **115**, 14149 (2011).

2 B. Santra, J. Klimeš, D. Alfè, A. Tkatchenko, B. Slater, A. Michaelides, R. Car, and M. Scheffler, Phys. Rev. Lett. **107**, 185701 (2011).

3 Éamonn D. Murray and G. Galli, Phys. Rev. Lett. **108**, 105502 (2012).

4 C. G. Salzmann, P. G. Radaelli, E. Mayer, and J. L. Finney, Phys. Rev. Lett. **103**, 105701 (2009).

5 W. Kohn and L. J. Sham, Phys. Rev. **140**, A1133 (1965).

6 J. Tao, J. P. Perdew, V. N. Staroverov, and G. E. Scuseria, Phys. Rev. Lett. **91**, 146401 (2003).

7 J. P. Perdew and W. Yue, Phys. Rev. B **33**, 8800 (1986).

8 J. Perdew, K. Burke, and M. Ernzerhof, Phys. Rev. Lett. **77**, 3865 (1996).

9 R. O. Jones and O. Gunnarsson, Rev. Mod. Phys. **61**, 689 (1989).

10 I. Lin, A. P. Seitsonen, M. Coutinho-Neto, I. Tavernelli, and U. Rothlisberger, J. Phys. Chem. B **113**, 1127 (2009).

11 Y. Zhang and W. Yang, Phys. Rev. Lett. **80**, 890 (1998).

12 J. Sun, M. Marsman, G. Csonka, A. Ruzsinszky, P. Hao, Y. Kim, G. Kresse, and J. P. Perdew, Phys. Rev. B **84**, 035117 (2011).

13 J. P. Perdew, A. Ruzsinszky, G. Csonka, L. A. Constantin, and J. Sun, Phys. Rev. Lett. **103**, 026403 (2009).

14 J. Sun, B. Xiao, and A. Ruzsinszky, J. Chem. Phys. **137**, 051101 (2012).

15 J. Sun, R. Haunschild, B. Xiao, I.W. Bulik,G.E. Scuseria, and J.P. Perdew, J. Chem. Phys. **138**, 044113 (2013).

16 J. Sun, B. Xiao, Y. Fang, R. Haunschild, P. Hao, A. Ruzsinszky, G.I. Csonka, G.E. Scuseria, and J.P. Perdew, arXiv:1303. 5688.

17 J. P. Perdew, S. Kurth, A. Zupan, and P. Blaha, Phys. Rev. Lett. **82**, 2544 (1999).

18 P. J. Feibelman, Phys. Chem. Chem. Phys. **10**, 4688 (2008).

19 S. Grimme, J. Comp. Chem. **27**, 1787 (2006).

20 M. Dion, H. Rydberg, E. Schröder, D. C. Langreth, and B. I. Lundqvist, Phys. Rev. Lett. **92**, 246401 (2004).

21 J. Klimeš, D. R. Bowler, and A. Michaelides, J. Phys. : Condensed Matter **22**, 022201 (2010).

22 J. Carrasco, B. Santra, J. Klimeš and A. Michaelides, Phy. Rev. Lett. **106**, 026101 (2011).

23 J. Klimeš, D. R. Bowler, and A. Michaelides, Phys. Rev. B **83**, 195131 (2011).

24 G. Kresse and J. Hafner, Phys. Rev. B **47**, 558 (1993).

25 G. Kresse and J. Furthmüller, Phys. Rev. B **54**, 11169 (1996).

26 D. R. Hamann, Phys. Rev. B **55**, R10157 (1997).

27 C. Lobban, J. L. Finney, and W. F. Kuhs, J. Chem. Phys **117**, 3928 (2002).

28 W.F. Kuhs, J.L. Finney, C. Vettier, and D.V. Bliss, J. Chem. Phys. **81**, 3612 (1984).

29 R. People and J. C. Bean, Appl. Phys. Lett. **47**, 322 (1985).

30 B. Vonnegut, J. Appl. Phys. **18**, 593 (1947).

31 J. P. Perdew and A. Zunger, Phys. Rev. B **23**, 5048 (1981).

32 S.L. Dong, Y. Wang, A.I. Kolesnikov, and J.C. Li, J. Chem. Phys. **109**, 235 (1998).

33 A. Tkatchenko and M. Scheffler, Phys. Rev. Lett. **102**, 073005 (2009).

34 A. Tkatchenko, R. A. DiStasio Jr., R. Car, and M. Scheffler, Phys. Rev. Lett. **108**, 236402 (2012).

35 A. Otero-de-la-Roza and V. Luaña, Comput. Phys. Comm. **182**, 1708 (2011).

36 A. Ruzsinszky, J.P. Perdew, J. Tao, G.I. Csonka, and J.M. Pitarke, Phys. Rev. Lett. **109**, 233203 (2012).

37 J.P. Perdew, A. Ruzsinszky, J. Sun, S. Glindmeyer, and G.I. Csonka, Phy. Rev. A **86**, 062714 (2012).

Figure captions

Fig. 1 Observed water ice phase diagram (Ref. [4]). One atmospheric pressure=101kPa =1.01×10^{-4}GPa.

Fig. 2 Percentage error of lattice constant for the ice-Ih on β-AgI lattice mismatch problem. Experimental lattice constants and mismatch value are taken from Ref. [18].

Fig. 3 (a) Relative lattice volume (ΔV_0) of the high-pressure ice-II and -VIII with respect to the lattice volume of ice-Ih (32.2 $Å^3/H_2O$ in MGGA_MS, for example), and (b) relative total energy (ΔU_0). (c) The energy versus volume curves of the ice-Ih and ice-VIII systems with MGGA_MS. The dotted line is the common tangent line obtained from the Birch-Murnaghan EOS. The slope of the straight line gives the transition pressure (P_{tr}). (d) Transition pressures (P_{tr}) from ice-Ih to the phases ice-II and -VIII. PBE0+vdW and reference DMC results and experimental values are taken from Ref. [2]. The calculated values do not include zero-point vibration effects. These effects are removed from the experimental total-energy changes, but not from the experimental equilibrium volumes.

Table

Table I Sublimation energies of ice-Ih, -II, -VIII (omitting zero-point energy effects). The total-energy differences ($\Delta U = U - U_{Ih}$, where $U = U_{II}$ or U_{VIII}) compared to ice-Ih (in parentheses) and the mean absolute relative error of the sublimation energy averaged over the three phases.

a: Experimental values are taken from Ref. [2], b: with zero-point energy contribution removed.

Unit: meV/H_2O	LSDA	PBE	revTPSS	TPSS+D2	revTPSS+vdW	MGGA_MS	optB88-vdW	optB86b-vdW	Expt[a,b]
Ice-Ih	943	636	570	720	644	602	696	706	610
Ice-II	896(47)	567(69)	507(63)	690(30)	630(14)	586(16)	699(-3)	701(5)	609(1)
Ice-VIII	813(130)	459(177)	423(147)	675(45)	569(75)	532(70)	670(26)	666(40)	577(33)
MARE (%)	47.5	10.5	16.7	16.1	3.5	4.3	15	15.4	

Figures

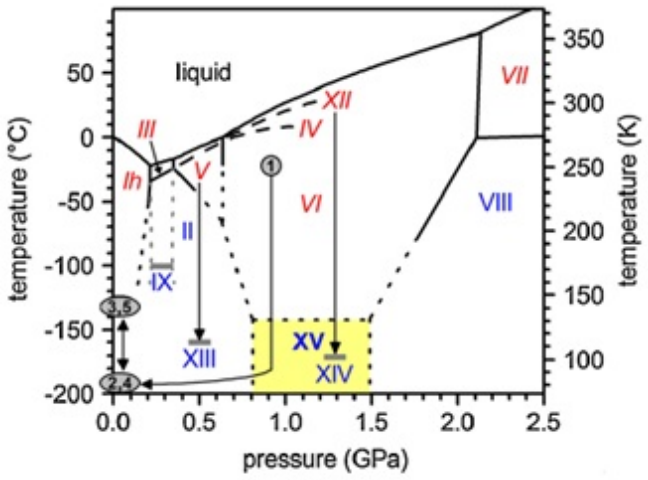

Fig. 1 Observed water ice phase diagram (Ref. [4]). One atmospheric pressure=101kPa =1.01x10^{-4}GPa.

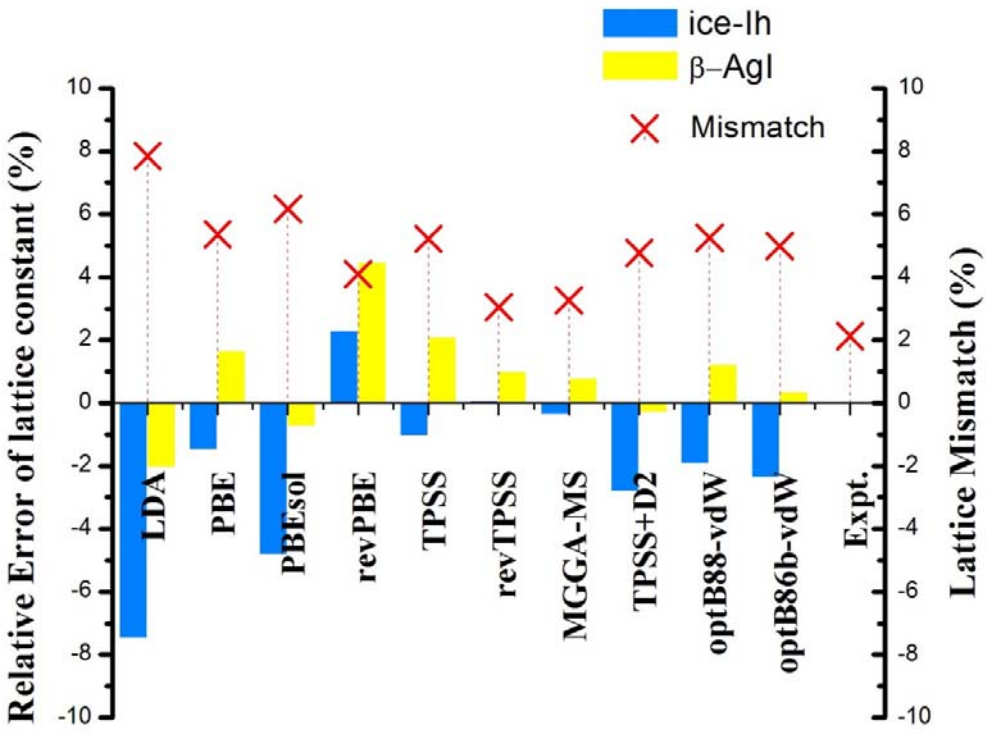

Fig. 2 Percentage error of lattice constant for the ice-Ih on β-AgI lattice mismatch problem. Experimental lattice constants and mismatch value are taken from Ref. [18].

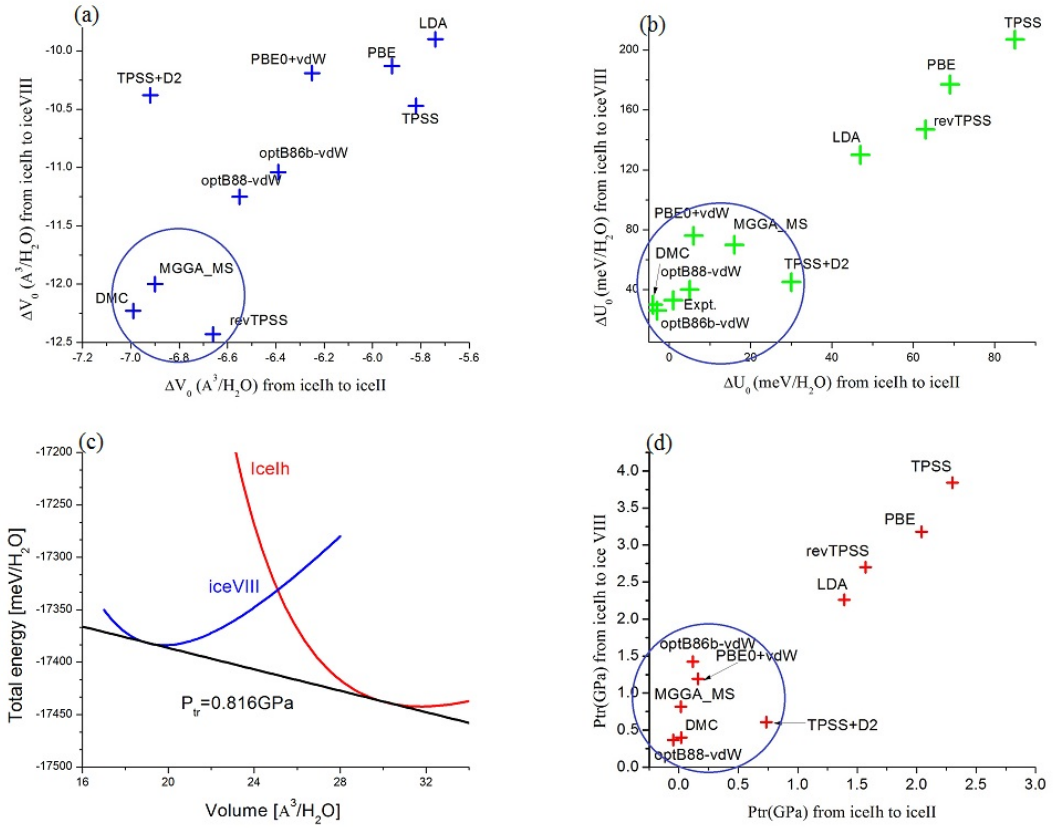

Fig. 3 (a) Relative lattice volume (ΔV_0) of the high-pressure ice-II and -VIII with respect to the lattice volume of ice-Ih (32.2 $Å^3/H_2O$ in MGGA_MS, for example), and (b) relative total energy (ΔU_0) (c) The energy versus volume curves of the ice-Ih and ice-VIII systems with MGGA_MS. The dotted line is the common tangent line obtained from the Birch-Murnaghan EOS. The slope of the straight line gives the transition pressure (P_{tr}). (d) Transition pressures (P_{tr}) from ice-Ih to the phases ice-II and -VIII. PBE0+vdW and reference DMC results and experimental values are taken from Ref. [2]. The calculated values do not

include zero-point vibration effects. These effects are removed from the experimental total-energy changes, but not from the experimental equilibrium volumes.